MDPI

Article

A Scalar Diagnostic for Empirical Score Alignment on Fisher Manifolds

Isaid Cornejo [1]

[1] Information Physics Institute (IPI); isaidcor@gmail.com
* Correspondence: isaidcor@gmail.com; Tel.: +52-56-4272-4979

Abstract

The Fisher–Rao metric provides the canonical geometric structure on statistical manifolds, yet empirical data often induce strong deviations from this geometry, manifesting through heavy-tailed spectra, dominant outlier modes, and effective dimensionality collapse in modern statistical models and neural networks. Existing metrics for quantifying these effects lack reparametrization invariance and do not directly compare empirical sensitivity to the intrinsic geometric baseline. We introduce a coordinate-free scalar diagnostic that measures the empirical deformation of Fisher geometry by contracting the empirical score covariance with the inverse Fisher metric, together with a rectified amplitude that isolates the excess-alignment sector. The associated alignment operator is shown to be diagonalizable with real non-negative eigenvalues, and the scalar diagnostic aggregates deviations through an invariant spectral identity that distinguishes empirical reinforcement from suppression. We validate the diagnostic across exponential families, Gaussian mixture models, and a trained neural network on MNIST, demonstrating that it captures equilibrium, suppression, and strong empirical reinforcement in a unified scalar signature. Reproducible code and figures are provided online.

Keywords: Fisher information; information geometry; empirical score covariance; alignment operator; spectral diagnostics; statistical manifolds; eigenvalue analysis; neural networks; high-dimensional statistics

MSC: 62B10; 62H12; 68T07

Received:
Revised:
Accepted:
Published:

Citation: Cornejo, I. Scalar Diagnostic for Empirical Score Alignment. *Entropy* **2025**, *1*, 0. https://doi.org/10.5281/zenodo.17810561

1. Introduction

The Fisher–Rao metric endows parametric statistical models with a canonical Riemannian structure that reflects infinitesimal statistical distinguishability [1–4]. Its geometric interpretation underlies classical asymptotic theory, natural gradient optimization [5,6], exponential-family structure [7,8], and the analysis of likelihood curvature in information geometry.

In practice, empirical data seldom match the model distribution exactly. Whenever the data-generating distribution $q(x)$ differs from the model $p(x|\theta)$, empirical score statistics become anisotropic, leading to heavy-tailed empirical Fisher matrices, dominant outlier eigenvalues, and effective dimensionality collapse. These phenomena are now well documented in high-dimensional models and deep networks [9–12].

Despite extensive spectral evidence, there remains no single, intrinsic, reparametrization-invariant-invariant scalar quantity that measures how empirical sensitivity

deviates from the Fisher baseline. Existing notions of effective dimensionality (e.g., participation ratio, effective rank, spectral entropy) are useful but do not compare empirical covariance to the intrinsic geometric expectation imposed by Fisher–Rao structure.

This work introduces a coordinate-free scalar diagnostic:

$$\mathcal{A}(\theta; q) = \mathrm{Tr}\Big(G^{-1}C\Big) - D,$$

together with a rectified amplitude

$$\phi(\theta; q) = \max\{\sqrt{\mathcal{A}}, 0\}.$$

We show that this diagnostic:

- measures the total empirical deviation from Fisher geometry,
- admits a spectral form $\mathcal{A} = \sum_i (\lambda_i - 1)$,
- distinguishes reinforcement from suppression through its sign,
- collapses high-dimensional spectral behavior into a single invariant.

The remainder of the paper is organized as follows. Section 2 reviews Fisher geometry and empirical covariance. Section 3 defines the alignment tensor and the scalar diagnostic. Section 4 develops the spectral representation. Section 5 characterizes equilibrium, suppression, and excess alignment. Section 6 presents empirical demonstrations. Section 7 discusses implications and limitations, and Section 8 concludes.

2. Background

Let $p(x|\theta)$ be a regular parametric statistical model with parameter $\theta \in \Theta \subset \mathbb{R}^D$. The score is defined as

$$v_i(x|\theta) = \partial_i \log p(x|\theta),$$

and the Fisher–Rao metric is

$$G_{ij}(\theta) = \mathbb{E}_p[v_i v_j]$$

as introduced in the foundational works of Fisher and Rao [1,2] and formalized in modern information geometry [3,4].

When empirical expectations are taken with respect to a distribution $q(x)$ that differs from $p(x|\theta)$, the empirical score covariance,

$$C_{ij}(\theta; q) = \mathbb{E}_q[v_i v_j],$$

generally deviates from the Fisher metric. This mismatch produces anisotropic empirical sensitivity.

In modern statistical models—particularly deep networks—empirical Fisher matrices often exhibit:

- heavy-tailed spectral decay,
- dominant outlier eigenvalues,
- effective dimensionality collapse,

phenomena that have been extensively documented in recent deep learning literature [9–12].

These effects motivate the need for principled, invariant diagnostics capable of characterizing empirical deviation from Fisher geometry.

3. The Alignment Tensor and Scalar Diagnostic

This section introduces the core geometric objects used throughout the paper: the empirical-alignment tensor, the scalar deviation diagnostic $\mathcal{A}(\theta; q)$, and its rectified amplitude $\phi(\theta; q)$. Together, these quantify how empirical sensitivity departs from the intrinsic Fisher–Rao structure [3,4].

3.1. Empirical Score Covariance

Empirical expectations with respect to the data distribution $q(x)$ define the empirical score covariance:

$$C_{ij}(\theta; q) = \mathbb{E}_q[\, v_i v_j \,]. \tag{1}$$

In general $C_{ij}(\theta; q)$ and $G_{ij}(\theta)$ need not coincide unless $q = p$, and even then equality may fail outside minimal exponential families [7,8].

The discrepancy between these two tensors captures the geometric deformation induced by the data.

3.2. The Alignment Tensor

We define the empirical-alignment tensor

$$\Delta_{ij}(\theta; q) = C_{ij}(\theta; q) - G_{ij}(\theta). \tag{2}$$

Interpretationally:

- $\Delta_{ij} = 0$ indicates Fisher-equivalent sensitivity.
- Positive eigenvalues of Δ correspond to reinforcement (empirical variance exceeding the Fisher baseline).
- Negative eigenvalues correspond to suppression.

Thus Δ_{ij} encodes direction-wise deviations of empirical sensitivity.

3.3. The Scalar Diagnostic

To obtain an invariant, coordinate-free quantity, we contract the alignment tensor with the inverse Fisher metric:

$$\mathcal{A}(\theta; q) := G^{ij}(\theta)\, \Delta_{ij}(\theta; q) = \mathrm{Tr}\Big(G^{-1}C\Big) - D. \tag{3}$$

[1]

This scalar diagnostic has three essential properties:

- **Reparametrization invariance**: it transforms as a scalar under smooth parameter transformations.
- **Signed structure**: $\mathcal{A} > 0$ indicates net reinforcement, whereas $\mathcal{A} < 0$ indicates net suppression.
- **Nontriviality**: $\mathcal{A} = 0$ does not imply $C_{ij} = G_{ij}$ unless the model satisfies strict exponential-family regularity [7].

[1] The equivalence between the contractions $G^{ij}(C_{ij} - G_{ij})$ and $\mathrm{Tr}(G^{-1}C) - D$ follows from the identity $G^{ij}G_{ij} = \delta^i_i = D$, which states that the trace of the Fisher metric equals the dimension of the parameter space. This holds in any coordinate system and does not assume a special parametrization.

3.4. Rectified Excess-Alignment Amplitude

In many settings only the *excess-alignment sector* is of interest—namely the directions along which empirical sensitivity exceeds the Fisher baseline. We therefore introduce the rectified amplitude:

$$\phi(\theta; q) = \max\{\sqrt{\mathcal{A}(\theta; q)}, 0\}. \tag{4}$$

By construction:

$$\phi = 0 \quad \Longleftrightarrow \quad \mathcal{A} \leq 0.$$

The quantity ϕ behaves analogously to an amplitude that captures the total strength of empirical reinforcement across all Fisher-orthonormal directions. The square-root scaling has a natural interpretation: since $\mathcal{A} = \sum_i (\lambda_i - 1)$ aggregates deviations additively, taking $\sqrt{\mathcal{A}}$ produces a Fisher-normalized magnitude rather than an energy-like sum. In this sense, ϕ acts as an amplitude associated with the subspace where $\lambda_i > 1$, providing a more interpretable measure of excess alignment intensity.

3.5. Signed Interpretation

The sign of $\mathcal{A}$ carries direct geometric meaning:

$$\begin{aligned} \mathcal{A} > 0: &\quad \text{net empirical reinforcement,} \\ \mathcal{A} = 0: &\quad \text{Fisher-equivalent sensitivity,} \\ \mathcal{A} < 0: &\quad \text{net empirical suppression.} \end{aligned}$$

Reinforcement corresponds to directions in which empirical curvature exceeds Fisher curvature, while suppression identifies damped or collapsed empirical modes.

These features become especially transparent through the spectral representation developed in Section 4.

4. Spectral Structure of the Alignment Operator

The scalar diagnostic $\mathcal{A}(\theta; q)$ becomes fully transparent when expressed through a natural mixed tensor that compares empirical and geometric sensitivity *direction by direction*. This section develops the spectral structure of that operator and establishes the key identity

$$\mathcal{A} = \sum_{i=1}^{D} (\lambda_i - 1),$$

which provides a complete and invariant summary of empirical deformation.

4.1. The Alignment Operator

Raising one index of the empirical covariance with the inverse Fisher metric defines the $(1,1)$ alignment operator:

$$H^i_{\ j}(\theta; q) := G^{ik}(\theta)\, C_{kj}(\theta; q). \tag{5}$$

Using the decomposition $C_{ij} = G_{ij} + \Delta_{ij}$, we obtain

$$H^i_{\ j} = \delta^i_{\ j} + G^{ik}\Delta_{kj}, \tag{6}$$

so that:

- $H = I$ under Fisher-equilibrium sensitivity,
- deviations from the identity encode empirical alignment,
- reinforcement and suppression manifest as eigenvalues above or below 1.

Although H need not be symmetric, it inherits strong spectral structure from the positive definiteness of the Fisher metric [3,4].

4.2. Diagonalizability and Symmetric Surrogate

Because G is positive definite, it admits a symmetric square root $G^{1/2}$ and its inverse $G^{-1/2}$ [3]. Writing

$$H = G^{-1}C \qquad \Longrightarrow \qquad H \sim G^{-1/2} C\, G^{-1/2},$$

we see that H is similar to the symmetric matrix $G^{-1/2} C\, G^{-1/2}$.

Consequences:

- all eigenvalues of H are real and non-negative,
- H is diagonalizable,
- the spectrum of H equals that of the symmetric surrogate.

Thus the empirical sensitivity deformation can be studied through a symmetric operator without altering the underlying geometry.

4.3. Eigenvalues as Sensitivity Ratios

Let $\lambda_1, \ldots, \lambda_D$ denote the eigenvalues of H, with eigenvectors $u^{(i)}$ normalized with respect to the Fisher metric:

$$G^{ij} u_i^{(k)} u_j^{(k)} = 1.$$

Inserting these eigenvectors into the relation $Hu = \lambda u$ yields:

$$\lambda = u^i C_{ij} u^j, \tag{7}$$

so each eigenvalue measures the empirical variance of the score *relative to* the Fisher–Rao expectation in that direction.

Interpretation:

- $\lambda_i > 1$ reinforced empirical sensitivity,
- $\lambda_i < 1$ suppressed empirical sensitivity,
- $\lambda_i = 1$ Fisher-equivalent sensitivity.

The spectrum of H therefore gives a direction-wise decomposition of empirical alignment on the statistical manifold.

4.4. Trace Identity and the Scalar Diagnostic

Taking the trace of the decomposition in Eq. (6) immediately gives

$$\mathrm{Tr}(H) = D + \mathrm{Tr}(G^{-1}\Delta).$$

Hence

$$\mathcal{A}(\theta; q) = \mathrm{Tr}(G^{-1}C) - D = \mathrm{Tr}(H) - D = \sum_{i=1}^{D} (\lambda_i - 1). \tag{8}$$

This establishes that $\mathcal{A}$ aggregates the total empirical deviation of H from the identity and that the rectified amplitude

$$\phi = \max\{\sqrt{\mathcal{A}}, 0\}$$

captures the *total strength of excess alignment*.

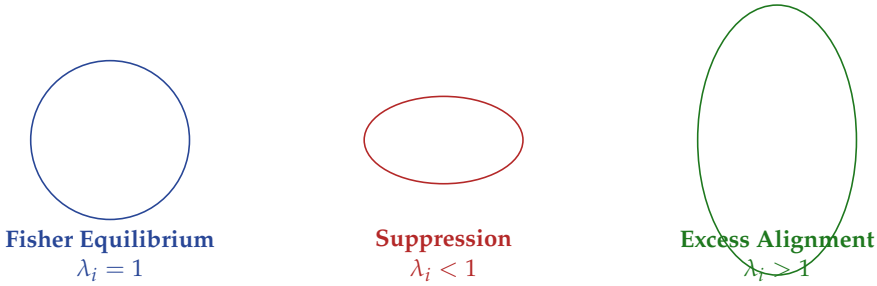

Figure 1. Geometric regimes of empirical alignment on a Fisher manifold. Equilibrium corresponds to isotropic curvature ($\lambda_i = 1$), suppression reflects contraction of sensitivity along one or more axes ($\lambda_i < 1$), and excess alignment corresponds to expansion beyond the Fisher baseline ($\lambda_i > 1$).

4.5. Relation to Dimensionality Measures

Although related to classical measures of effective dimensionality such as the participation ratio and effective rank, the diagnostic $\mathcal{A}$ differs in three key ways:

- it compares empirical sensitivity directly against the Fisher baseline,
- it is signed, distinguishing suppression and reinforcement,
- it is a scalar invariant under reparametrization.

Thus $\mathcal{A}$ offers a complementary perspective to spectral summaries commonly used in high-dimensional statistics and deep learning [9–12].

5. Alignment Regimes

The spectrum of the alignment operator $H = G^{-1}C$ naturally partitions the behavior of empirical sensitivity into three fundamental regimes: *equilibrium*, *suppression*, and *excess alignment*. Each regime corresponds to a distinct empirical deformation of Fisher–Rao geometry and has clear geometric and statistical interpretation.

We summarize these regimes below before turning to empirical demonstrations.

5.1. Fisher Equilibrium

A model is in Fisher equilibrium at θ when

$$\lambda_i(\theta; q) = 1 \quad \text{for all } i.$$

In this regime, empirical score covariance matches the geometric expectation set by the Fisher metric. The alignment tensor vanishes,

$$\Delta_{ij} = 0, \qquad \mathcal{A} = 0, \qquad \phi = 0,$$

and the empirical sensitivity landscape is isotropic in Fisher-orthonormal coordinates.

This regime occurs when $q = p$ in minimal exponential families [7,8] or when empirical and model curvature coincide despite mild model misspecification. Gaussian families (with mean and variance parameters) provide canonical examples.

5.2. Suppression Regime

The suppression regime corresponds to

$$\lambda_i < 1 \quad \text{for one or more eigenvalues.}$$

Here empirical variance falls *below* the Fisher–Rao baseline, indicating that the data distribution q concentrates sensitivity into a lower-dimensional tangent subspace than predicted by the model.

Key signatures:

$$\mathcal{A} < 0, \qquad \phi = 0,$$

reflecting a net contraction of empirical sensitivity.

Suppression manifests in models with heavy-tailed likelihood structure, sharp modes, or symmetry-induced collapse. The Laplace family provides a simple example: even under $q = p$, empirical curvature does not match Fisher curvature, yielding slight suppression [13].

Geometrically, suppression corresponds to a flattening of the empirical local quadratic structure relative to the intrinsic Fisher geometry.

5.3. Excess Alignment

Excess alignment occurs when

$$\exists\, i : \lambda_i > 1,$$

and is characterized by empirical reinforcement along one or more Fisher-orthonormal directions.

In this regime:

$$\mathcal{A} > 0, \qquad \phi = \sqrt{\mathcal{A}}.$$

Large outlier eigenvalues reflect strong anisotropy in empirical sensitivity, where q emphasizes fluctuations aligned with specific directions of the tangent space. Gaussian mean-shift perturbations yield mild excess alignment; neural networks often display extreme instances, with $\lambda_{\max} \gg 1$ indicating dominant reinforcement modes [9–11].

Geometrically, excess alignment corresponds to an empirical reshaping of the local geometry into a directionally stretched structure relative to the Fisher metric.

5.4. Mixed Regimes and Directional Structure

In many practical cases, empirical spectra contain both suppressed and reinforced directions:

$$\lambda_{i_1} < 1, \qquad \lambda_{i_2} > 1.$$

Such mixed regimes occur frequently in:

- misspecified models,
- mixture models,
- deep networks,
- hierarchical generative models.

The scalar diagnostic $\mathcal{A}$ measures the *net* deviation across all directions, while the full spectrum reveals the balance between reinforcement and suppression.

5.5. Summary

The three alignment regimes encode qualitatively different empirical geometric behaviors:

Regime	Scalar Signature	Interpretation
Equilibrium	$\mathcal{A} = 0$	Empirical curvature matches the Fisher expectation.
Suppression	$\mathcal{A} < 0$	Empirical sensitivity is contracted relative to the Fisher baseline.
Excess Alignment	$\mathcal{A} > 0$	Empirical reinforcement; increased anisotropy relative to Fisher geometry.

These regimes will be illustrated concretely through empirical experiments in Section 6.

6. Empirical Validation Across Statistical Models

This section presents the empirical behavior of the scalar diagnostic $\mathcal{A}(\theta; q)$ and its rectified amplitude $\phi(\theta; q)$ across four families of models: Gaussian, Laplace, Gaussian mixtures, and a trained neural network on MNIST. Each experiment follows the same computational pipeline:

1. Compute the Fisher information matrix G.
2. Compute the empirical covariance C under the data distribution q.
3. Form the Fisher-normalized operator

$$H = G^{-1/2} C\, G^{-1/2},$$

   which is symmetric and positive semidefinite.
4. Compute its eigenvalues λ_i.
5. Evaluate the scalar diagnostic

$$\mathcal{A} = \sum_{i=1}^{D} (\lambda_i - 1), \qquad \phi = \max\{\sqrt{\mathcal{A}}, 0\}.$$

All experiments were generated using the reproducible suite in `src/experiments/`, with figures automatically produced via:

```
python -m src.generate_figures
```

The figures included below correspond exactly to the outputs stored in `paper/figures/generated/`.

6.1. Gaussian Family: Equilibrium and Mean-Shift Misalignment

The Gaussian model provides the simplest instance of Fisher equilibrium and controlled deviation from it. Under $q = p$, the empirical covariance matches the Fisher metric, yielding eigenvalues $\lambda_i \approx 1$ and thus $\mathcal{A} \approx 0$.

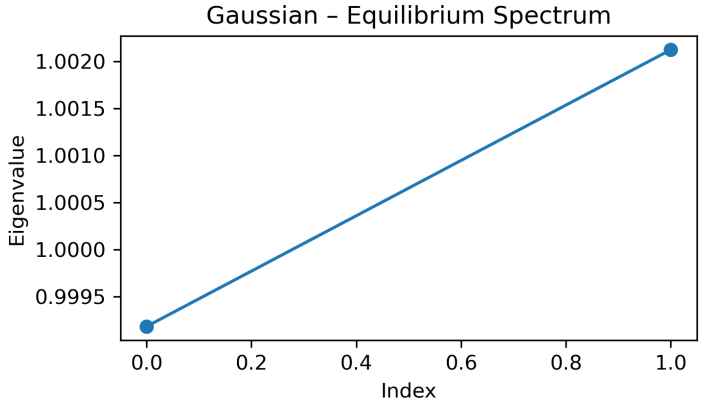

Figure 2. Eigenvalue spectrum of the alignment operator for the Gaussian model under Fisher equilibrium. Both eigenvalues satisfy $\lambda_i \approx 1$, producing $\mathcal{A} \approx 0$ and $\phi = 0$.

A simple mean shift induces asymmetric deformation of empirical sensitivity: one direction becomes reinforced ($\lambda > 1$) while the other is suppressed ($\lambda < 1$). This produces $\mathcal{A} > 0$ and a nonzero coherence amplitude.

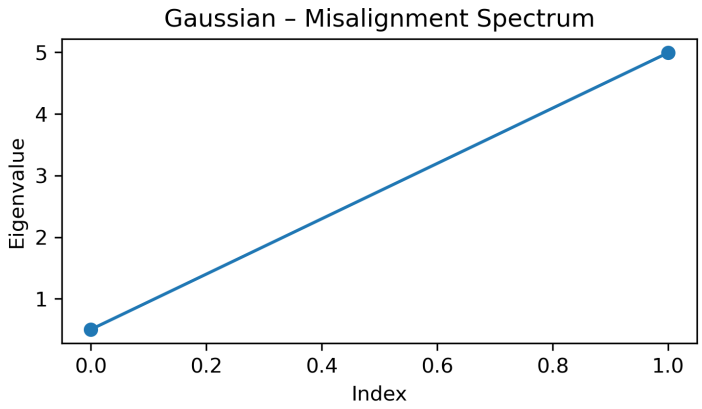

Figure 3. Gaussian misalignment via mean-shift. One eigenvalue is reinforced ($\lambda \approx 5$) while the other is suppressed, yielding $\mathcal{A} > 0$ and $\phi > 0$.

6.2. Laplace Family: Structural Suppression

The Laplace model is not a minimal exponential family, so even under $q = p$ the empirical covariance deviates slightly from the Fisher metric [13]. This produces mild suppression ($\lambda_i < 1$) and therefore $\mathcal{A} < 0$.

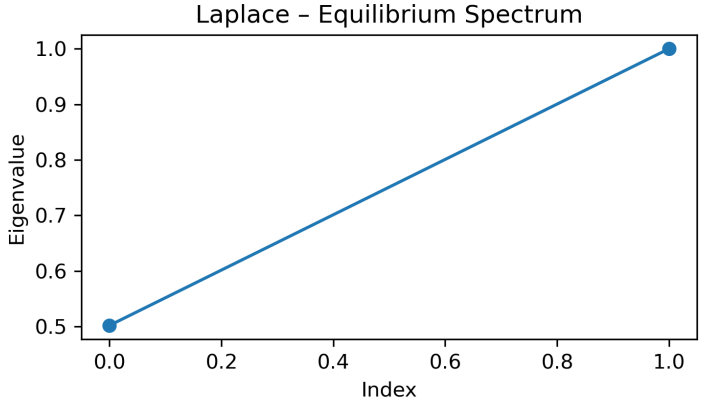

Figure 4. Laplace equilibrium. Even when $q = p$, the non-exponential-family structure induces $\lambda_i < 1$ and $\mathcal{A} < 0$, reflecting structural suppression.

Under a shifted data distribution, both eigenvalues fall further below 1, demonstrating clear global suppression and vanishing coherence amplitude: $\phi = 0$.

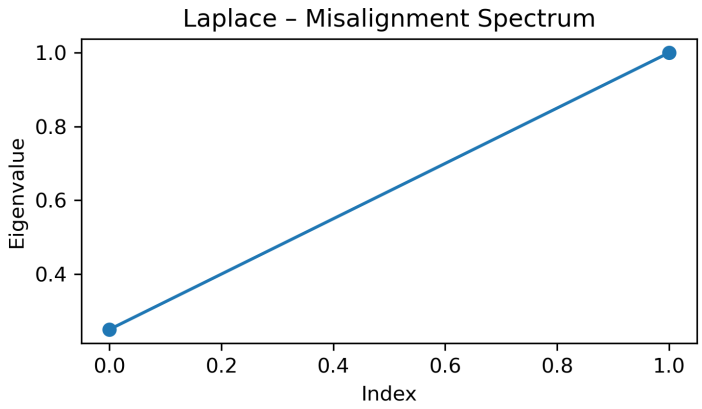

Figure 5. Laplace misalignment. Both eigenvalues satisfy $\lambda_i < 1$, yielding $\mathcal{A} < 0$ and $\phi = 0$, characteristic of a global suppression regime.

6.3. Gaussian Mixture Model: Multimodal Reinforcement

Gaussian mixtures introduce multimodality, leading to anisotropic empirical curvature and mild outlier eigenvalues even under equilibrium conditions [14].

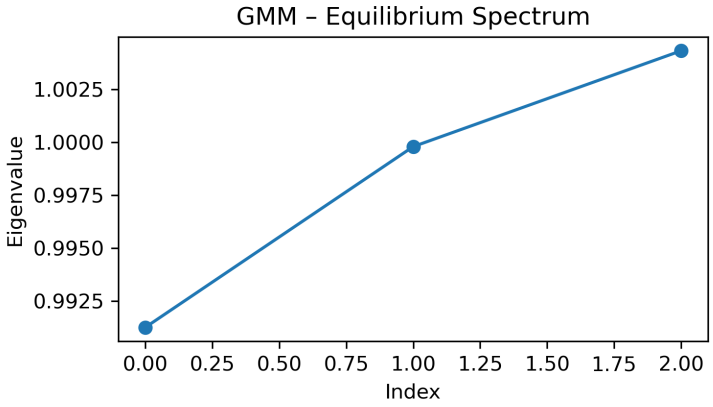

Figure 6. GMM equilibrium. Small deviations around $\lambda_i \approx 1$ arise from sampling variability and multimodal structure, with $\mathcal{A} \approx 0$.

When the mixture is misaligned relative to the data, the empirical covariance acquires clear reinforcement modes ($\lambda > 1$) while other directions remain suppressed, producing a net positive scalar diagnostic.

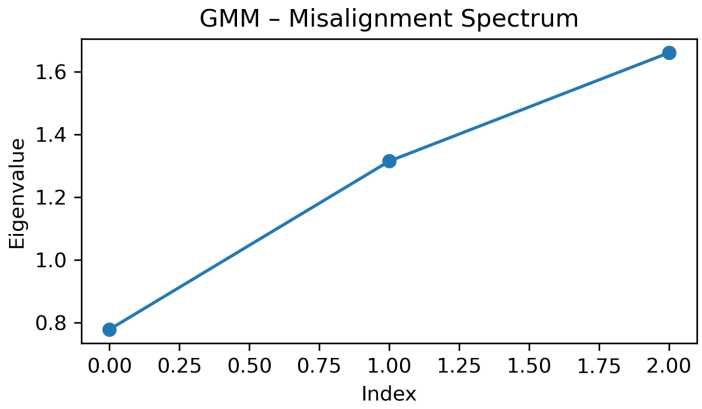

Figure 7. GMM misalignment. Multimodality induces reinforced directions ($\lambda > 1$) and suppressed ones ($\lambda < 1$), yielding $\mathcal{A} > 0$.

6.4. Neural Network on MNIST: Strong Empirical Anisotropy

A fully connected network trained on MNIST [15] exhibits a dramatically anisotropic alignment spectrum. The largest eigenvalue satisfies $\lambda_{\max} \gg 1$, indicating extremely reinforced empirical curvature. Most remaining eigenvalues collapse near zero, reflecting effective dimensionality reduction [9–11].

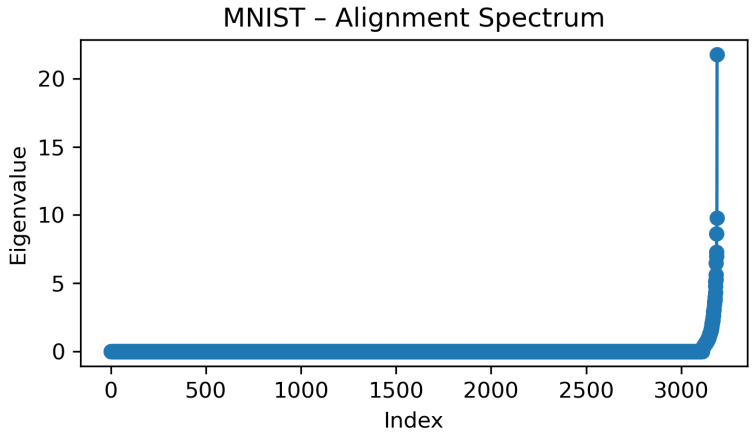

Figure 8. Alignment spectrum of a trained MNIST MLP. The presence of a large outlier eigenvalue ($\lambda_{\max} \gg 1$) indicates strong empirical reinforcement, while the bulk collapses toward 0. This produces a large positive scalar diagnostic $\mathcal{A}$ and a correspondingly strong coherence amplitude.

6.5. Summary

Across all tested families—Gaussian, Laplace, mixture models, and neural networks—the scalar diagnostic $\mathcal{A}$ and its rectified amplitude ϕ accurately capture the empirical deformation of Fisher geometry:

- $\mathcal{A} \approx 0$ under Fisher equilibrium,
- $\mathcal{A} < 0$ in structural or global suppression regimes,
- $\mathcal{A} > 0$ when empirical reinforcement emerges,
- large $\mathcal{A}$ in deep models with strong curvature outliers.

A consolidated numerical summary is provided in the table at the end of the paper.

7. Discussion

The scalar diagnostic introduced in this work provides a unified framework for quantifying empirical deviations from Fisher–Rao geometry. Its spectral representation in terms

of the eigenvalues of $H = G^{-1}C$ allows for a transparent geometric and statistical interpretation: empirical reinforcement corresponds to $\lambda_i > 1$, suppression corresponds to $\lambda_i < 1$, and the deviation from equilibrium aggregates into the single invariant $\mathcal{A} = \sum_i (\lambda_i - 1)$.

7.1. Interpretation of Empirical Alignment

The interpretation of alignment through the Fisher-normalized spectrum reveals how empirical data shape the effective sensitivity of a model:

- Reinforced directions correspond to strong curvature induced by the data distribution, often reflecting dominant modes, coherent structures, or training-induced specialization in neural networks [9–12].
- Suppressed directions correspond to collapsed or constrained sensitivity, arising either from structural properties of the model (as in the Laplace family) or from data distributions that reduce empirical variability.

In this sense, the scalar diagnostic captures not only the magnitude but also the *balance* between these two opposing geometric tendencies.

7.2. Comparison to Existing Notions of Dimensionality

Traditional measures of effective dimensionality—participation ratio, spectral entropy, effective rank—summarize properties of a covariance or Hessian matrix but do not compare empirical sensitivity to the model's intrinsic geometric structure. The diagnostic $\mathcal{A}$ differs fundamentally in that it quantifies *empirical deformation relative to Fisher–Rao geometry*, making it invariant under reparametrization and applicable across a broad range of models.

Moreover, $\phi = \max\{\sqrt{\mathcal{A}}, 0\}$ isolates the excess-alignment sector, which is often of particular interest in detecting dominant curvature modes, optimization instabilities, or critical transitions during learning.

7.3. Implications for Optimization and Learning Dynamics

The presence of reinforced directions ($\lambda_i \gg 1$) suggests that empirical curvature concentrates strongly along a small number of directions, a behavior commonly associated with:

- rapid convergence along principal gradient directions,
- stiff optimization dynamics,
- the emergence of low-dimensional effective subspaces,
- sensitivity to initialization or perturbations.

Conversely, suppressed directions ($\lambda_i \ll 1$) correspond to regions where empirical curvature is weaker than geometric expectations, hinting at flat directions, redundancies in parameterization, or underconstrained degrees of freedom.

The scalar diagnostic therefore provides a compact summary of how learning or sampling reshapes the geometric landscape of a model.

7.4. Limitations and Scope

Several limitations should be kept in mind:

- Estimating G and C can be challenging in high dimensions, often requiring regularization, subsampling, or approximate score estimation.
- The scalar diagnostic summarizes only the trace structure of the alignment operator and does not capture the full eigenstructure of H. It should therefore be interpreted alongside (or informed by) spectral information when available.
- $\mathcal{A} = 0$ does not imply $q = p$; rather, it indicates that the empirical and geometric traces agree. Only in minimal exponential families does vanishing $\mathcal{A}$ correspond to exact Fisher equilibrium [7,8].

Despite these limitations, the diagnostic retains conceptual simplicity while capturing essential geometric information spanning suppression, equilibrium, and reinforcement regimes.

Trace cancellation.

A vanishing diagnostic, $\mathcal{A} = 0$, enforces only that the *trace* of the alignment operator equals that of the identity. Reinforced and suppressed directions may cancel:

$$\sum_{i=1}^{D}(\lambda_i - 1) = 0 \quad \not\Rightarrow \quad \lambda_i = 1 \ \ \forall i.$$

Thus $\mathcal{A} = 0$ may occur even when $C \neq G$ and the empirical geometry remains anisotropic. Minimal exponential families are the only class for which $\mathcal{A} = 0$ guarantees full Fisher equilibrium, since no cancellation across directions is possible.

Scalability considerations.

The computation of the alignment operator $H = G^{-1}C$ requires solving a linear system with the Fisher metric and, in high-dimensional models, computing (or approximating) its eigenvalues. While this is tractable for the low- and moderate-dimensional settings considered here, large-scale neural networks may require stochastic approximations, low-rank projections, or Lanczos-type methods for estimating the dominant eigenvalues of H. Because $\mathcal{A}$ depends only on the trace of H, randomized trace estimators or Hutchinson-type methods offer practical scalable alternatives in very high dimensions.

7.5. Outlook

The scalar diagnostic may have broader implications in:

- monitoring the evolution of curvature during training,
- characterizing transitions between learning phases,
- informing natural gradient or curvature-aware optimization methods,
- studying generalization via curvature-based metrics,
- analyzing implicit models where score estimation is approximate.

The empirical experiments included in this work demonstrate that the diagnostic remains stable, interpretable, and informative across classical models, mixture models, and deep neural networks.

Future work may explore alignment flows, dynamical equations for alignment, connections to information geometry in statistical physics, and the behavior of $\mathcal{A}$ in large-scale, high-dimensional learning systems.

8. Conclusion

This work introduced a reparametrization-invariant scalar diagnostic for quantifying empirical deviation from Fisher–Rao geometry. By expressing the alignment operator $H = G^{-1}C$ in a Fisher-normalized form, we showed that its spectrum admits real, non-negative eigenvalues whose deviation from unity captures reinforced and suppressed empirical sensitivity. The resulting scalar invariant,

$$\mathcal{A} = \sum_{i=1}^{D}(\lambda_i - 1), \qquad \phi = \max\{\sqrt{\mathcal{A}}, 0\},$$

provides a concise geometric summary of these effects.

Across a range of models—from exponential families [7,8] to mixture models [14] to trained neural networks—the diagnostic exhibited consistent behavior aligned with

theoretical expectations: $\mathcal{A} \approx 0$ under equilibrium, $\mathcal{A} < 0$ under suppression, and $\mathcal{A} > 0$ whenever empirical reinforcement was present. Deep networks, in particular, displayed strong anisotropic curvature characterized by large outlier eigenvalues and large positive values of $\mathcal{A}$ [9–12].

The scalar diagnostic sits alongside, but distinct from, existing measures of effective dimensionality, offering a geometric perspective centered on deviation from Fisher curvature rather than absolute spectral shape. Its invariance under reparametrization and ease of computation make it suitable for monitoring learning dynamics, analyzing curvature-induced phase transitions, or informing curvature-aware optimization.

Future avenues include extending the diagnostic to implicit or score-based models, studying dynamical flows of empirical alignment during training, exploring high-dimensional asymptotics, and connecting alignment behavior to generalization and robustness in modern learning systems.

All experiments and figures in this work are fully reproducible. Code is available at github.com/isaidcornejo/coherence-field.

Summary Table of Spectral Regimes

Table 1. Summary of empirical alignment regimes across models.

Model	Regime	λ	$\mathcal{A}$	ϕ	Interpretation
MNIST MLP	Excess	$\gg 1, \sim 0$	$\gg 1$	$\gg 1$	Strong dimensional collapse; curvature-dominant mode.
GMM (Equilibrium)	Eq.	~ 1	0	0	Geometric stability.
GMM (Misaligned)	Excess	(0.78, 1.32, 1.66)	0.76	0.87	Moderate directional reinforcement.
Gaussian (Equilibrium)	Eq.	(0.999, 1.002)	0.0013	0.036	Near-perfect Fisher equilibrium.
Gaussian (Mean-shift)	Misalign.	(0.52, 5.00)	3.52	1.88	One dominant reinforced mode.
Laplace (Equilibrium)	Sub-align	(0.50, 1.00)	-0.50	0	Structural suppression (non-exponential family).
Laplace (Misaligned)	Sub-align	(0.25, 1.00)	-0.75	0	Full collapse along one direction.

Author Contributions: Conceptualization, I.C.; methodology, I.C.; software, I.C.; validation, I.C.; formal analysis, I.C.; investigation, I.C.; resources, I.C.; data curation, I.C.; visualization, I.C.; writing—original draft preparation, I.C.; writing—review and editing, I.C. The author has read and agreed to the published version of the manuscript.

Funding: This research received no external funding.

Institutional Review Board Statement: Not applicable.

Informed Consent Statement: Not applicable.

Data Availability Statement: All code and reproducibility materials supporting this study are openly available in the GitHub repository: https://github.com/isaidcornejo/coherence-field.

Acknowledgments: Not applicable.

Conflicts of Interest: The author declares no conflict of interest.

References

1. Fisher, R.A. On the Mathematical Foundations of Theoretical Statistics. *Philosophical Transactions of the Royal Society A* **1922**, *222*, 309–368. https://doi.org/10.1098/rsta.1922.0009.
2. Rao, C.R. Information and the Accuracy Attainable in the Estimation of Statistical Parameters. *Bulletin of the Calcutta Mathematical Society* **1945**, *37*, 81–89.
3. Amari, S.i.; Nagaoka, H. *Methods of Information Geometry*; Translations of Mathematical Monographs, American Mathematical Society, 2000. https://doi.org/10.1007/978-1-4612-0167-1.
4. Amari, S.i. *Information Geometry and Its Applications*; Springer, 2016. https://doi.org/10.1007/978-3-319-56478-4.
5. Amari, S.i. Natural Gradient Works Efficiently in Learning. *Neural Computation* **1998**, *10*, 251–276. https://doi.org/10.1162/089976698300017746.
6. Martens, J. New Insights and Perspectives on the Natural Gradient Method. *arXiv:1412.1193* **2014**.
7. Brown, L.D. *Fundamentals of Statistical Exponential Families*; Institute of Mathematical Statistics, 1986.
8. Wainwright, M.J.; Jordan, M.I. Graphical Models, Exponential Families, and Variational Inference. *Foundations and Trends in Machine Learning* **2008**, *1*, 1–305. https://doi.org/10.1561/2200000001.
9. Papyan, V.; Han, X.Y.; Donoho, D.L. Prevalence of Neural Collapse During the Terminal Phase of Deep Learning Training. *PNAS* **2020**, *117*, 24652–24663. https://doi.org/10.1073/pnas.2010055117.
10. Sagun, L.; Bottou, L.; LeCun, Y. Eigenvalues of the Hessian in Deep Learning: Singularity and Beyond. *arXiv:1611.07476* **2016**.
11. Ghorbani, B.; Krishnan, S. An Investigation into Neural Net Hessians. *arXiv:1810.05487* **2018**.
12. Nakkiran, P.; et al. Deep Double Descent: Where Bigger Models and More Data Hurt. *ICLR* **2020**.
13. Kotz, S.; Kozubowski, T.; Podgórski, K. The Laplace Distribution and Generalizations. *Springer Series in Statistics* **2001**. https://doi.org/10.1007/b97636.
14. McLachlan, G.; Peel, D. *Finite Mixture Models*; Wiley, 2000.
15. LeCun, Y.; Bottou, L.; Bengio, Y.; Haffner, P. Gradient-Based Learning Applied to Document Recognition. *Proceedings of the IEEE* **1998**, *86*, 2278–2324. https://doi.org/10.1109/5.726791.